SPi	Journal Code	Article ID	Dispatch: 06-MAR-18	CE:
	MET	1716	No. of Pages: 18	ME:

Received: 28 February 2017 | Revised: 13 November 2017 | Accepted: 26 January 2018

DOI: 10.1002/met.1716

Meteorological Applications RMetS

RESEARCH ARTICLE

Sensitivity of initial-condition and cloud microphysics to the forecasting of monsoon rainfall in South Asia

Md Safat Sikder | Faisal Hossain

Department of Civil and Environmental Engineering, University of Washington, Seattle, WA, USA

Correspondence
F. Hossain, Department of Civil and Environmental Engineering, University of Washington, Seattle, WA 98195, USA.
Email: fhossain@uw.edu

Funding information
National Aeronautics and Space Administration, Grant/Award number: NNX16AO68H; NASA Earth and Space Fellowship, Grant/Award number: NNX16AO68H; NASA, Grant/Award number: NNX15AC63G

The main objective of this study is to assess the impact of using different initialization techniques and cloud microphysics of a numerical atmospheric model to improve the forecasting of Indian summer monsoon rainfall (ISMR). A total of six intense precipitation events over the Ganges–Brahmaputra–Meghna (GBM) and Indus River basins were tested to identify the most suitable combination of parameterization and initialization techniques. The global forecast system (GFS)-based numerical weather prediction (NWP) forecast fields were dynamically downscaled by the mesoscale model of weather research and forecasting (WRF). The performance of four types of initial conditions with three cloud microphysics was assessed using a model resolution of up to 9 km. A main conclusion is that the model initialized using hot start in the study involves more uncertainty, probably due to poor-quality data assimilation, and it cannot exceed the performance of cold-start initialization. The study findings provide evidence that the finer resolution initial condition is promising in higher resolution models. In the case of cloud microphysics, the performance of WRF single moment 5 class (WSM5) was sufficient for South Asian monsoon systems within this scale of the model resolution. The findings provide a general guideline for flood forecasters for the WRF model set-up for forecasting the ISMR from publicly available GFS-based NWP forecast fields.

KEYWORDS
forecasting, Indian summer rainfall, monsoon, numerical weather prediction, weather research and forecasting, floods

1 | INTRODUCTION

The economies of South Asia are predominantly agrarian with a significant dependence on monsoon rainfall (Molden, 2007). The high population density in most of the South Asian river basins (e.g. the Ganges, Brahmaputra and Indus) makes the situation more complex (Kale, 2012). Flooding in such river basins causes substantial damage to lives and properties. For example, a widespread flood in the Ganges basin caused by monsoon rainfall in 2007 killed over 2,000 people and displaced about 20 million (Dulal, 2014). Therefore, understanding and prediction of monsoon rainfall are very important for this region.

Predicting monsoon rainfall is complicated because of the irregular characteristics of the monsoon in the tropical cycle (Dwivedi, Mittal, & Goswami, 2006). Numerous studies have been conducted to understand the monsoon system better. Such studies have explored how to predict ahead of time (hereafter referred to as "forecasting") the timing and intensity of the Indian summer monsoon rainfall (ISMR). Many of these studies typically use a global numerical weather prediction (NWP) model as the primary tool (e.g. Bhaskaran, Jones, Murphy, & Noguer, 1996; Medina, Houze Jr, Kumar, & Niyogi, 2010; Srinivas et al., 2013). Such a NWP is perhaps the only plausible option for forecasting rainfall by piecing together the fundamental building blocks of weather-prediction variables that lead to precipitation, i.e. humidity (mass), pressure/wind speed (momentum) and temperature (energy).

A quantitative precipitation forecast (QPF) using NWP models has not yet reached the required accuracy at the regional scale (Cuo, Pagano, & Wang, 2011; Kalnay, 2003; Nam, Mai, Udo, & Mano, 2014). The QPF is challenging because of inadequate observational data, as well as the improper physical representation of the precipitation (hereafter used interchangeably with "rainfall") process in models due to lack of knowledge (Ebert, 2001; Vaidya, 2006; Yucel & Onen, 2014). The uncertainty in the NWP model-derived precipitation can be introduced from several sources: model physical parameterization, initial condition (IC) or computational precision (Rakesh, Singh, Pal, & Joshi, 2009). The simulation uncertainty can be reduced by advancing the physical parameterization, applying better numerical techniques and improving state estimation of the IC *via* data assimilation (Jang & Hong, 2014). The QPF is also sensitive to model resolution (Roberts, Cole, Forbes, Moore, & Boswell, 2009), model domain size (Bray, Han, Xuan, Bates, & Williams, 2011), model downscaling ratio (Liu, Bray, & Han, 2012), and initial and boundary data (Kumar, Kishtawal, & Pal, 2015). Moreover, the suitable model parameterization, resolution and boundary can vary by region, season and storm type, and often needs to be fine-tuned separately (Sikka & Rao, 2008).

Model parameterization is the most studied feature of NWP models. Many studies have conducted sensitivity tests of different model parameterizations on real storm events (e.g. Alam, 2014; Rakesh, Singh, Pal, & Joshi, 2007; Ratnam & Cox, 2006). Past studies have shown that the QPF is directly related to the cloud microphysics (MP) and cumulus parameterization (CP) of high-resolution NWP models (Sikder & Hossain, 2016). The MP explicitly resolves water vapour, cloud and precipitation processes in the model. Put simply, the MP scheme is responsible for cloud and ice formation, their evolution and eventual fallout as precipitation. The CP is used in coarse-resolution NWP models (> 10 km), when the MP scheme cannot capture the fine-scale convective events explicitly (Hsiao et al., 2013; Roberts & Lean, 2008). The CP scheme is responsible for sub-grid-scale convective precipitation in NWP models. Numerous studies reported that the ISMR is sensitive to the choice of CP scheme (e.g. Sikder & Hossain, 2016; Srinivas, Prasad, Rao, Baskaran, & Venkatraman, 2015). Many of these studies found that the Betts–Miller–Janjic (BMJ) CP scheme (Janjic, 1994) performs reasonably well in the case of ISMR (e.g. Kumar, Dudhia, & Bhowmik, 2010; Mukhopadhyay, Taraphdar, Goswami, & Krishnakumar, 2010).

Besides the physical parameterization, the QPF also depends on the accuracy of the IC (Bei & Zhang, 2007). The errors in representing the IC are eventually amplified by the chaotic nature of the primitive equations of weather models (Lorenz, 1963). Therefore, several approaches can be introduced into the NWP models to quantify and reduce the uncertainty in representing the IC. One approach is to quantify the uncertainty in the IC with the use of model ensembles (e.g. Durai & Bhardwaj, 2013; Georgakakos et al., 2014). In the ensemble approach, the model is initialized with multiple perturbations of the IC to reduce sensitivity to a single realization of the IC. Data assimilation is another approach (Kalnay, 2003) that has been used frequently to improve the ISMR forecasts (e.g. Raju, Parekh, Kumar, & Gnanaseelan, 2015; Rakesh, Singh, Yuliya, Pal, & Joshi, 2009; Routray et al., 2010; Sowjanya, Kar, Routray, & Mali, 2013).

If one had to prioritize key issues, then the short-term rainfall forecast can be considered most sensitive primarily to model parameterization and the IC. In this study, the sensitivity of both NWP factors to the ISMR forecast was investigated. The motivation of such a study is twofold. From a societal standpoint, any improvement in the QPF translates directly to greater benefits in flood forecasting or water supply management at short lead times (from days to weeks). From a computational standpoint for the weather modeller, exploring the impact of the IC demands revisiting the chaotic nature of the weather system vis-à-vis its physical modelling complexity.

This study is particularly skewed towards the latter motivation of exploring the IC. The natural intuition is to expect any improvement in representation of the IC to translate directly as improved skill in the forecasting of rainfall. However, given the chaotic nature of weather and the further computational complexities of today's NWP models, just how consistent is the impact of the IC on forecast accuracy? To the best of the authors' knowledge, such a question has not been answered previously for the monsoon-driven climate regime. In order to elucidate the weather-scale features of a storm system, dynamic downscaling of the coarse-resolution NWP output through a higher-resolution cloud-resolving model is the common strategy employed in this study. In scientific terminology first defined by Castro, Pielke Sr, and Leoncini (2005), the study focuses on type 1 downscaling tailored to short-term weather prediction and that involves the representation of the IC.

The main objective of this study is, therefore, to assess the impact of using different model-initialization techniques (for IC) and cloud MP to improve rainfall forecasting of the ISMR and guide the flood forecaster. In addition to the above question, an overarching question asked here is: Is it possible to improve the precipitation forecast over South Asian river basins affected by the monsoon using the appropriate model initialization techniques and cloud microphysics?

2 | THE WRF MODEL AND BOUNDARY DATA

The weather research and forecasting (WRF) model V3.7.1 was used for dynamic downscaling (type 1) of the coarse-resolution global NWP weather forecast and to generate a high-resolution precipitation forecast over South Asia. The WRF is a mesoscale cloud-resolving NWP model, which is the successor of the MM5 model. It uses non-hydrostatic Euler equations, which are fully compressible in nature. The WRF offers various features such as advanced dynamics, physics and numerical schemes. For computation, the model uses Arakawa-C grid staggering for horizontal discretization, and a second- or third-order Runge–Kutta integration scheme for time separation. It uses a terrain-flowing pressure-co-ordinate system. Thus, the upper boundary of the model is maintained by a constant pressure level. For a further description of the WRF physics and dynamics, see Skamarock et al. (2008).

The WRF model can be initialized with the boundary from the various global NWP models such as the global forecast system (GFS), the coupled forecast system (CFS) and regional NWP models such as the North American mesoscale model (NAM). These large-scale NWP model forecast output data are used to generate the initial and lateral boundary condition for the WRF model. In this study, the GFS outputs were used as the WRF initial and boundary condition. The GFS is developed by the National Oceanic and Atmospheric Administration (NOAA) and produces global-scale weather forecast every 6 hr up to 16 days of lead time. As a publicly available service for the world, the GFS is ideal for short-term weather prediction applications, particularly in South Asia where economic resources are constrained. The spatial and temporal resolutions vary with lead time. For the first 10 days of lead time, the GFS provides forecasts for every 3 hr, and the outputs are available at 0.25, 0.5, 1.0 and 2.5° resolution. Historical data of this model have been available at a 0.5° resolution since October 2006. The lead time of the historical data varies with time. The 0.5° GFS model outputs were used to run the WRF in this study.

At certain times of the day (four times), the GFS model is initiated with the latest available observed data to generate a real-time operational forecast. A significant amount of observed data are available within a few hours after the operational GFS model is started. The National Centers for Environmental Prediction (NCEP) runs the same model (i.e. the GFS) later, with all available observed data and using the same data-assimilation technique. This product is known as the NCEP final analysis, often termed the GFS-FNL. Since the model starts after a few hours of the operational GFS model, it does not generate the forecast but produces the hindcast. This final analysis usually contains 10% more observed data in the representation of the IC than the standard "quick-view" GFS forecast. These data are available at 1 and 6 hr resolution. Recently, the NCEP has started to distribute finer analysis data using the same procedure of the GFS-FNL described above. This high-resolution NCEP final analysis uses the global data assimilation system (GDAS) such as GFS-FNL and termed the NCEP GDAS final analysis (hereafter GDAS-FNL) at the University Corporation for Atmospheric Research (UCAR) data portal. These GDAS-FNL data are available at 0.25° resolution. Like the GFS-FNL, the GDAS-FNL is initiated every 6 hr, with 10–15% more observed data than the GFS forecast. Therefore, these hindcast products are expected to be more accurate than the normal GFS forecast. Thus, for monsoonal flood-forecasting operations for lead times up to one week, there is no reason why the GFS-FNL and GDAS-FNL cannot be used as model ICs in a real-world environment.

3 | STUDY REGION AND METHODOLOGY

The Indian summer monsoon (ISM) covers most of the Indian subcontinent. The Ganges–Brahmaputra–Meghan (GBM) river basin system of this region, which drains out through Bangladesh to the Bay of Bengal, was selected for this study. This system covers about 1.7 million km^2, where at least 750 million people reside (FAO, 2011). Another selected large river basin within the ISM regime was the Indus basin. The area of this river basin is 1.12 million km^2, where about 200 million people live. In total, about 1 billion people live in the river basins of the GBM and Indus combined and are directly or indirectly affected by the ISMR.

The earlier model set-ups of the GBM and Indus basin used by Sikder and Hossain (2016) were used as a starting point in this study. Set-ups for both basins have two modelling domains. The outer domain (D01) covers almost the same area of the Indian subcontinent and Indian Ocean in both set-ups (Figure 1). The inner domain (D02) covers a slightly larger area than the extent of the river basin. In both model set-ups, the resolutions of D01 and D02 are 27 and 9 km respectively. Furthermore, an analysis extent within the D02 was selected in order to evaluate the accuracy of the precipitation forecast. The analysis extent within the GBM basin was divided into two segments due to strong gradients of precipitation within this large basin system. The heavy rainy area within the GBM basin covers the humid subtropical region of the eastern Indian subcontinent (Figure 1a). The less rainy area covers mainly the semi-arid region of the mid-western Indian subcontinent. For the Indus basin, the analysis extent covers almost the entire basin area (Figure 1b).

Sikder and Hossain (2016) had already identified three appropriate MP–CP combinations for the monsoon climate regime of South Asia. They reported that three different MP schemes work well with the BMJ CP scheme in both the GBM and Indus basins in a hindcast mode. These MP

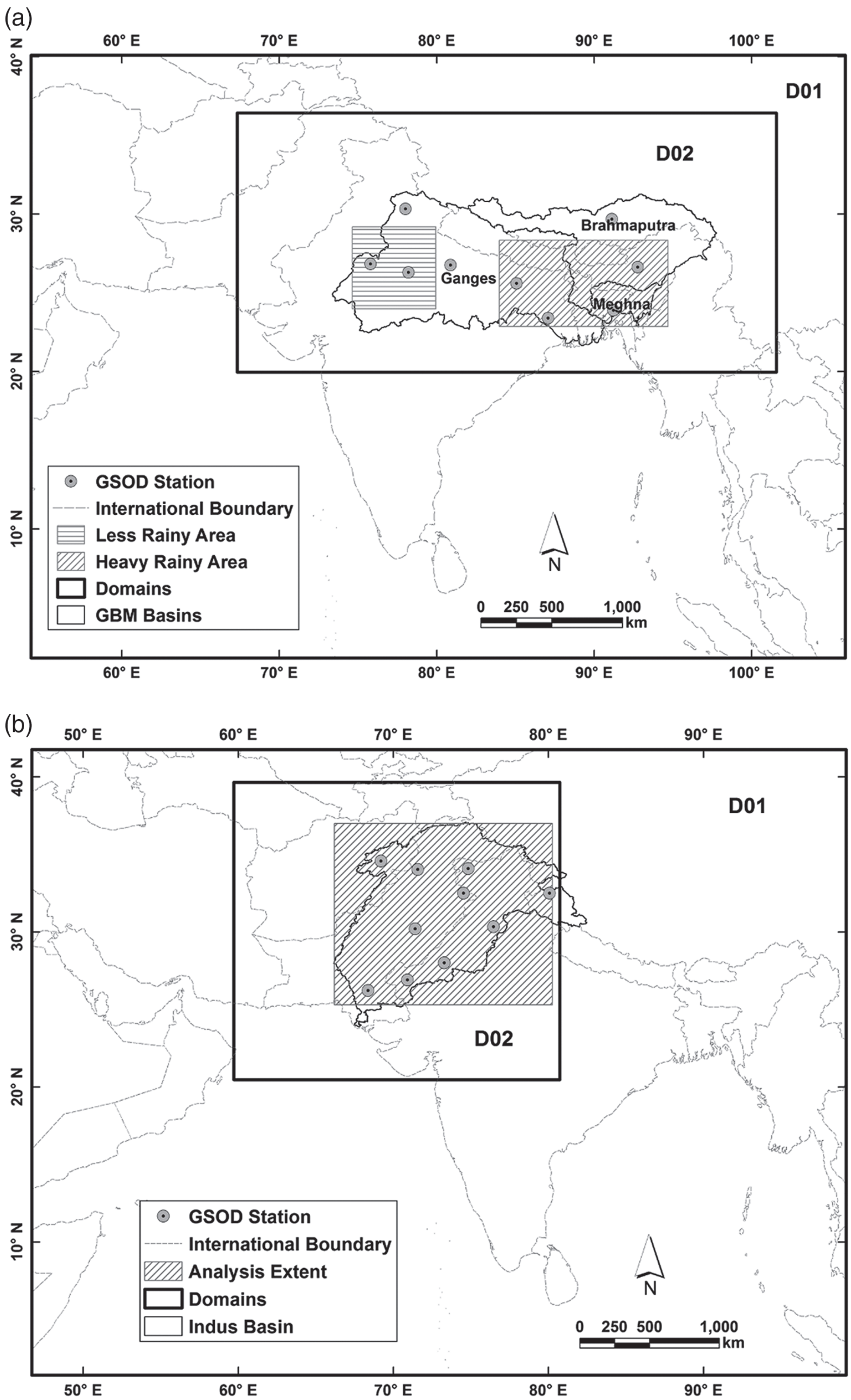

FIGURE 1 Weather research and forecasting (WRF) model domains and analysis of the extents of (a) the Ganges–Brahmaputra–Meghna (GBM); and (b) the Indus basin along with the selected Global Summary of the Day of the National Climatic Data Center (NCDC-GSOD) stations used for the performance evaluation of simulated temperature and wind speed

schemes are the WRF single moment 5 class (WSM5) (Hong, Dudhia, & Chen, 2004), the WRF single moment 6 class (WSM6) (Hong & Lim, 2006) and the Thompson scheme (TS) (Thompson, Field, Rasmussen, & Hall, 2008). In this study, the sensitivity of these three likely best MP schemes was assessed in terms of forecasted precipitation. Hereafter, the MP schemes are denoted by their abbreviation (e.g. WSM6). Other model parameterizations used in this study are the BMJ CP scheme (Janjic, 1994), the Yonsei University (YSU) planetary boundary layer scheme (Hong, Noh, & Dudhia, 2006), the unified Noah land surface model land-surface scheme (Tewari et al., 2004), the MM5 similarity surface layer scheme (Zhang & Anthes, 1982), the Dudhia short wave (Dudhia, 1989) and the RRTM long wave (Mlawer, Taubman, Brown, Iacono, & Clough, 1997) radiation schemes.

Besides the sensitivity test of the MP schemes in the WRF forecast, the performance of four different WRF model initialization techniques was tested in this study. In the first experiment case, the traditional "cold-start" technique was used to initiate the WRF model using the GFS forecast (e.g. Givati, Lynn, Liu, & Rimmer, 2012). The IC of the WRF model was directly taken from the GFS forecast in this case. The second case was also a cold-start set-up, but the first-hour GFS forecast data were replaced by the GFS-FNL data which are expected to represent a more accurate IC given the higher number of assimilated observations. Thus, the IC of the model is derived from the GFS-FNL and simulation was continued using the GFS forecast data as the model boundary. Exclusion of the first 6 hr simulation output of a cold-start model is a common practice used to eliminate the model "spin-up" time error. Although the first two cases involved cold-start initialization, the spin-up effect was not considered in this study to evaluate the advantages of other initialization techniques.

The next two cases were based on a "warm start" (often called a "hot start") approach (e.g. Jankov, Gallus Jr, Segal, & Koch, 2007). The output of a one-day pre-simulated WRF model was used to initiate the WRF forecast model in these cases. In this way, the uncertainty related to model instability during the so-called spin-up time is expected to be reduced. The GFS-FNL data were used as the initial and boundary condition for this one-day pre-simulation (i.e. hindcast), since they contain more observed data than the operational GFS. Thereafter, the WRF forecast model was initiated with the restart generated from this hindcast model, and continued with the GFS forecast data as the boundary condition in the third experiment case. The last experimental case was almost similar to the third experimental case. The only difference was the first-hour GFS forecast data were replaced by the GFS-FNL data in the WRF forecast simulation. Therefore, the last case is the fusion of the second and third experimental cases. These four experiment cases are denoted here by IC and a serial number denoting the experimental case. Hereafter, the IC1 means the first experiment case to initiate the WRF model; and IC2, IC3 and IC4 the second, third and fourth experimental cases respectively.

The IC might have an effect on the forecasted temperature and wind speed, which directly influence the precipitation and other forecasted variables. Thus, the sensitivity of different IC approaches in forecasted daily average wind speed at 10 m height, and the maximum and minimum temperature at 2 m height were assessed. Furthermore, the sensitivity of the spatial resolution of the IC data was tested to understand better the IC approaches used. To do so, the IC2, IC3 and IC4 test cases were simulated again, but using the GDAS-FNL instead of the GFS-FNL data. Finally, a straightforward comparison between the GFS, GFS-FNL and GDAS-FNL was conducted to assess the performance of generating the WRF IC using these different products.

Six different events associated with a heavy rainy day over the GBM and Indus basin during the monsoon period were selected (Table 1). Each event was simulated up to five days of lead time, and the simulation period varied with events by 7–10 days. Twelve different test cases are possible (three MP × four IC) in each event. Because it is computationally challenging to simulate all these six events using all 12 combinations, the events were simulated for a few of the microphysics–initial condition (MP–IC) combinations. Only the GBM 2007 and Indus 2010 events were simulated for all 12 MP–IC combinations. The selected combinations are listed in Table 1.

TABLE 1 Selected events and lead time along with simulated microphysics–initial condition (MP–IC) combinations

Basin	Event	Simulation period (peak rainy day)	Simulated forecast generated with a 1–5 day lead time	IC	MP WSM5	MP WSM6	MP TS
GBM	GBM 2007	July 20–26, 2007 (July 26)	July 24–26, 2007	IC1	×	×	×
				IC2	×	×	×
				IC3	×	×	×
				IC4	×	×	×
	GBM 2015.1	August 11–20, 2015 (August 20)	August 16–20, 2015	IC1			×
				IC2			×
				IC3			×
				IC4	×	×	×
	GBM 2015.2	August 21–30, 2015 (August 30)	August 26–30, 2015	IC4	×	×	×
Indus	Indus 2007	June 22–28, 2007 (June 28)	June 26–28, 2007	IC1	×	×	×
	Indus 2010	July 22–29, 2010 (July 28)	July 26–29, 2010	IC1	×	×	×
				IC2	×	×	×
				IC3	×	×	×
				IC4	×	×	×
	Indus 2012	September 1–9, 2012 (September 9)	September 5–9, 2012	IC4	×	×	×

Notes: Crosses indicate a selected IC–MP combination.
GBM, Ganges–Brahmaputra–Meghna; IC, initial condition; MP, microphysics; TS, Thompson scheme; WSM, single moment class.

4 | HISTORY AND BACKGROUND OF THE SELECTED PRECIPITATION EVENTS

4.1 | The GBM 2007 event

The year 2007 was a widespread flood year in South Asia. Several countries, including Bangladesh, Bhutan, India and Nepal, were affected severely from this flood event. The event was one of the major five flood events in Bangladesh within a 20 year return period (the last recorded similar event was in 1987) (Mirza, 2011). The precipitation amount over the Brahmaputra and Meghna river basins in July 2007 was higher than any other month of the previous two years (Islam, Haque, & Bala, 2010). In this study, a particular day of the event was selected: July 26, 2007, when the 24 hr-accumulated areal-averaged precipitation (from the Global Summary of the Day of the National Climatic Data Center — NCDC-GSOD) exceeded 26 mm within the heavy rainy area of the GBM basin (Figure 2a).

4.2 | The GBM 2015 event

The year 2015 was also a substantial flood year for the GBM basin. Two events were selected when the 24 hr-accumulated-areal average precipitation (from the NCDC-GSOD) within the heavy rainy domain exceeded 20 mm. The first event was on August 20 and the second was on August 30. 2015 (Figure 2c, e). The first and second events of 2015 are denoted here as GBM 2015.1 and GBM 2015.2 respectively.

4.3 | The Indus 2007 event

Pakistan was also severely affected by the South Asian floods in 2007. Its coastal area was affected by a cyclone in late June, followed by heavy monsoon precipitation in July–August. The cyclone disappeared on June 26. Immediately after the cyclone, a heavy rainfall event affected the North-West Frontier and Punjab (World Bank, 2007). The peak was observed within the Indus basin on June, 28 (Figure 2b), when the 24 hr-accumulated basin average rainfall was over 10 mm (from the NCDC-GSOD).

4.4 | The Indus 2010 event

The 2010 flood event in the Indus basin was one of the most severe in the recent history of Pakistan (Paulikas & Rahman, 2015). The flood was caused by heavy monsoon precipitation in late July. An unusual wind and pressure anomaly on that day conveyed moisture into the northwestern part of the country and caused heavy rainfall (Houze Jr, Rasmussen, Medina, Brodzik, & Romatschke, 2011). Wang, Davies, Huang, and Gillies (2011) claimed that the anomalies observed during the event were not intermittent, and this abnormal circulation was a part of the long-term trend of the monsoon. However, precipitation of this event intensified on July 28 (Figure 2d). The 24 hr-accumulated basin-average precipitation was over 17 mm on that day (from the NCDC-GSOD).

4.5 | The Indus 2012 event

During 2012, monsoon precipitation within the Indus basin was moderate until August. Rainfall rapidly intensified during the first half of September and caused severe flooding in Pakistan. The precipitation peaked between September 6–11 in the Punjab and Sindh provinces of Pakistan (Memon, Muhammad, Rahman, & Haq, 2015). The maximum 24 hr-accumulated areal-averaged precipitation within the basin area was on September 9 (Figure 2f), and exceeded 11 mm (from the NCDC-GSOD).

5 | REFERENCE DATA AND ANALYSIS TECHNIQUE

Two sets of reference data were used to evaluate the performance of the WRF-forecasted precipitation. A gridded reference data set was used to determine the ability of the model to capture precipitation in the spatial direction. Tropical rainfall measuring mission (TRMM) product 3B42V7 was used as the gridded reference data source. These daily data are available at 0.25° resolution. Details of this product are described by Huffman (2013). Another data set was used to evaluate the accuracy of the model to estimate the amount of precipitation. The GSOD data set provided by the NCDC was used for this purpose. This *in situ* station-based data set is available through the World Meteorological Organization (WMO). The Thiessen polygon approach was applied to determine the areal average precipitation within the analysis extents of the GBM and Indus basins. Figure 2 shows the locations of the available stations within the study areas and their associated Thiessen polygons in the GBM and Indus basin respectively. The same data source (i.e. the NCDC-GSOD) was used for the performance evaluation of simulated daily maximum temperature, minimum temperature and average wind speed. Based on the data availability, a total of nine and 10 stations for temperature and wind speed were used for the GBM and Indus basin respectively. The stations were selected carefully to cover the entire basin as well as the different climate regime. The locations of these stations are shown in Figure 1.

The model performance metrics in this study were divided into two parts, as done by Liu et al. (2012). Four categorical metrics were used to understand model accuracy to determine rainfall in the spatial direction. These metrics are the probability of detection (POD), frequency bias index (FBI), false alarm ratio (FAR) and critical success index (CSI). They were calculated with respect to the gridded

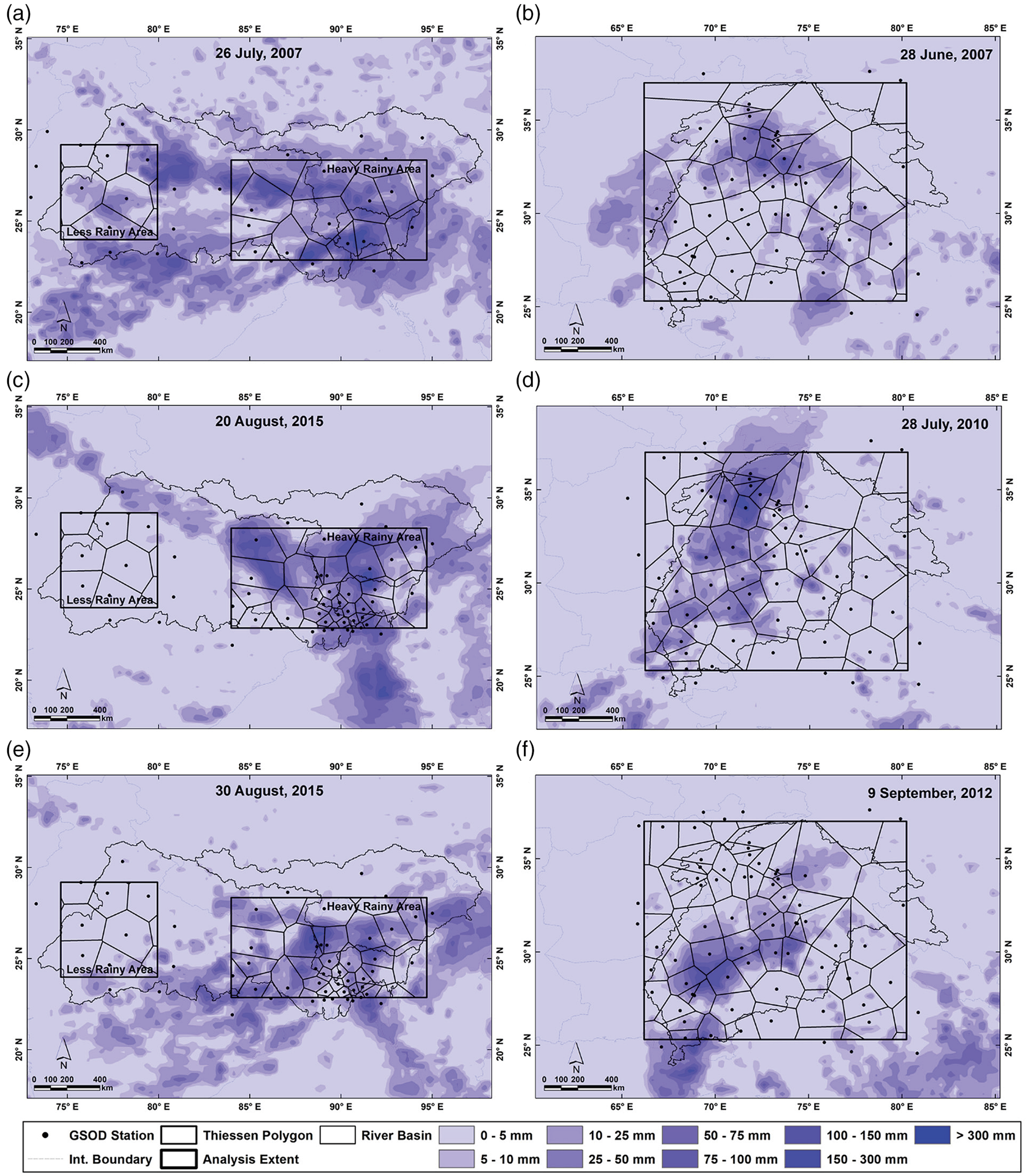

Color online, B&W in print

FIGURE 2 Selected intense precipitation events (tropical rainfall measuring mission (TRMM) 3B42V7) in the Ganges–Brahmaputra–Meghna (GBM) (a, c, e) and Indus basin (b, d, f) along with the available Global Summary of the Day of the National Climatic Data Center (NCDC-GSOD) station within the analysis extents and their associated Thiessen polygons [Color figure can be viewed at wileyonlinelibrary.com]

reference data (i.e. the TRMM). The categorical metrics were calculated based on the contingency table of precipitation (Table 2).

TABLE 2 Contingency table for precipitation analysis

Simulated/observed	$\text{Rain}_{\text{observed}}$	$\text{No Rain}_{\text{observed}}$
$\text{Rain}_{\text{simulated}}$	RR (hit)	RN (false rain)
$\text{No Rain}_{\text{simulated}}$	NR (miss)	NN (correct negative)

The equations for calculating the average categorical metrics are:

$$\text{POD} = \frac{1}{n}\sum_{i=1}^{n}\frac{RR_i}{RR_i + NR_i} \tag{1}$$

$$\text{CSI} = \frac{1}{n}\sum_{i=1}^{n}\frac{RR_i}{RR_i + RN_i + NR_i} \tag{2}$$

$$\text{FAR} = \frac{1}{n}\sum_{i=1}^{n}\frac{RN_i}{RR_i + RN_i} \tag{3}$$

$$\text{FBI} = \frac{1}{n}\sum_{i=1}^{n}\frac{RR_i + RN_i}{RR_i + NR_i} \tag{4}$$

where n is the number of time steps multiplied by the number of grid cells. The POD is the probability of success to detect rainfall with respect to all observed rainfall. The CSI, often termed as "Theta score," also represents the same characteristics as the POD, but with respect to all observed rainfall as well as the unwanted rainfall generated by the simulation. Both metrics ranged from 0 to 1, where 1 is for the ideal case. The FAR indicates the probability of false rainfall generated by the simulation with respect to all rainfall generated by the model. The perfect score for the FAR is 0. All three metrics (POD, CSI, FAR) do not consider the bias of forecasted rainfall. The FBI was used to detect the trend (i.e. under- or overestimation) of the simulated precipitation with respect to the observed data. The FBI ranged from 0 to infinity, where 1 is the ideal score. Any value smaller than or greater than 1 indicates that the simulation is under- or overestimating the event respectively.

Similarly, three continuous metrics were used to evaluate the ability of the model to estimate the amount of precipitation: the root mean squared error (RMSE), mean bias error (MBE) and standard deviation (SD). All were evaluated with respect to the areal averaged *in situ* measured rainfall data (i.e. the NCDC-GSOD).

The equations of the continuous metrics are:

$$\text{RMSE} = \sqrt{\frac{1}{n}\sum_{i=1}^{n}\left(R_{\text{sim}} - R_{\text{obs}}\right)^2} \tag{5}$$

$$\text{MBE} = \frac{1}{n}\sum_{i=1}^{n}\left(R_{\text{sim}} - R_{\text{obs}}\right) \tag{6}$$

$$\text{SD} = \sqrt{\frac{1}{n-1}\sum_{i=1}^{n}\left(R_{\text{sim}} - R_{\text{obs}} - \text{MBE}\right)^2} \tag{7}$$

where n is the number of time steps; R_{sim} and R_{obs} are the simulated and observed areal averaged precipitation within the analysis extent respectively; the RMSE and SD represent the amount of error but not the direction of the error with respect to the observes; and the MBE indicates the cumulative error as well as the direction of the simulated rainfall bias. The MBE can be any real number. A negative or positive MBE indicates that the model is under- or overestimating the amount of precipitation respectively.

Evaluating the performance of the simulated rainfall derived from different sets of combinations is difficult when using seven different metrics. Therefore, a single skill score that can combine the characteristics of the seven metrics is useful. A skill score (called the unified score) defined previously by Sikder and Hossain (2016) was used. For

TABLE 3 Equations of rescaled metrics

Rescaled error metrics	Threshold
$\text{POD}_r = \text{POD}$	
$\text{FBI}_r = (\text{FBI}_{max} - \text{FBI})$; when $\text{FBI} > 1$	$\text{FBI}_{max} = 2$
$\text{FBI}_r = \text{FBI}$; when $\text{FBI} < 1$	
$\text{FAR}_r = 1 - \text{FAR}$	
$\text{CSI}_r = \text{CSI}$	
$\text{MBE}_r = 1 - \text{MBE}/\text{MBE}_{max}$; when $\text{MBE} > 0$	$\text{MBE}_{max} = 15$
$\text{MBE}_r = 1 - \text{MBE}/\text{MBE}_{min}$; when $\text{MBE} < 0$	$\text{MBE}_{min} = -15$
$\text{RMSE}_r = (1 - \text{RMSE}/\text{RMSE}_{max})$	$\text{RMSE}_{max} = 15$
$\text{SD}_r = (1 - \text{SD}/\text{SD}_{max})$	$\text{SD}_{max} = 15$

convenience, a description of this skill score is now provided. The unified score is the simple average of all seven error metrics. Here all error metrics have the same weight. At first, these seven metrics were rescaled in a range between 0 and 1. The equations used for the rescaling are shown in Table 3. Here the threshold values of the FBI, MBE and RMSE were set based on the maxima and minima of these metrics found in this study. All the rescaled metrics (denoted with subscript "r") range from 0 to 1, where 1 is the ideal value. Thereafter, the average of all rescaled error metrics was taken and named the unified score, ranging from 0 to 1, with the perfect score being 1:

$$\text{Unified score} = \left(\frac{\text{POD}_r + \text{CSI}_r + \text{FAR}_r + \text{FBI}_r + \text{RMSE}_r + \text{MBE}_r + \text{SD}_r}{7}\right) \tag{8}$$

Another skill score was used to understand the performance of the spatial distribution of the forecasted precipitation. Named the "spatial extent score," it was used to evaluate the model performance of a single-day event, where it was not possible to calculate the continuous metrics. This score was calculated by taking the average of only the rescaled categorical metrics. Thus, it mainly represents model performance in the spatial direction. The range and ideal value of this skill score is the same as for the unified score:

$$\text{Spatial extent score} = \left(\frac{\text{POD}_r + \text{CSI}_r + \text{FAR}_r + \text{FBI}_r}{4}\right) \tag{9}$$

Performance of the simulated daily maximum temperature, minimum temperature and average wind speed were evaluated using the average MBE and RMSE of all stations within the basins.

6 | RESULTS AND DISCUSSION

In the GBM basin, the analysis was carried out in two different locations to observe the WRF precipitation forecast performance in different climate regimes. The selected intense precipitation events were located within the heavy

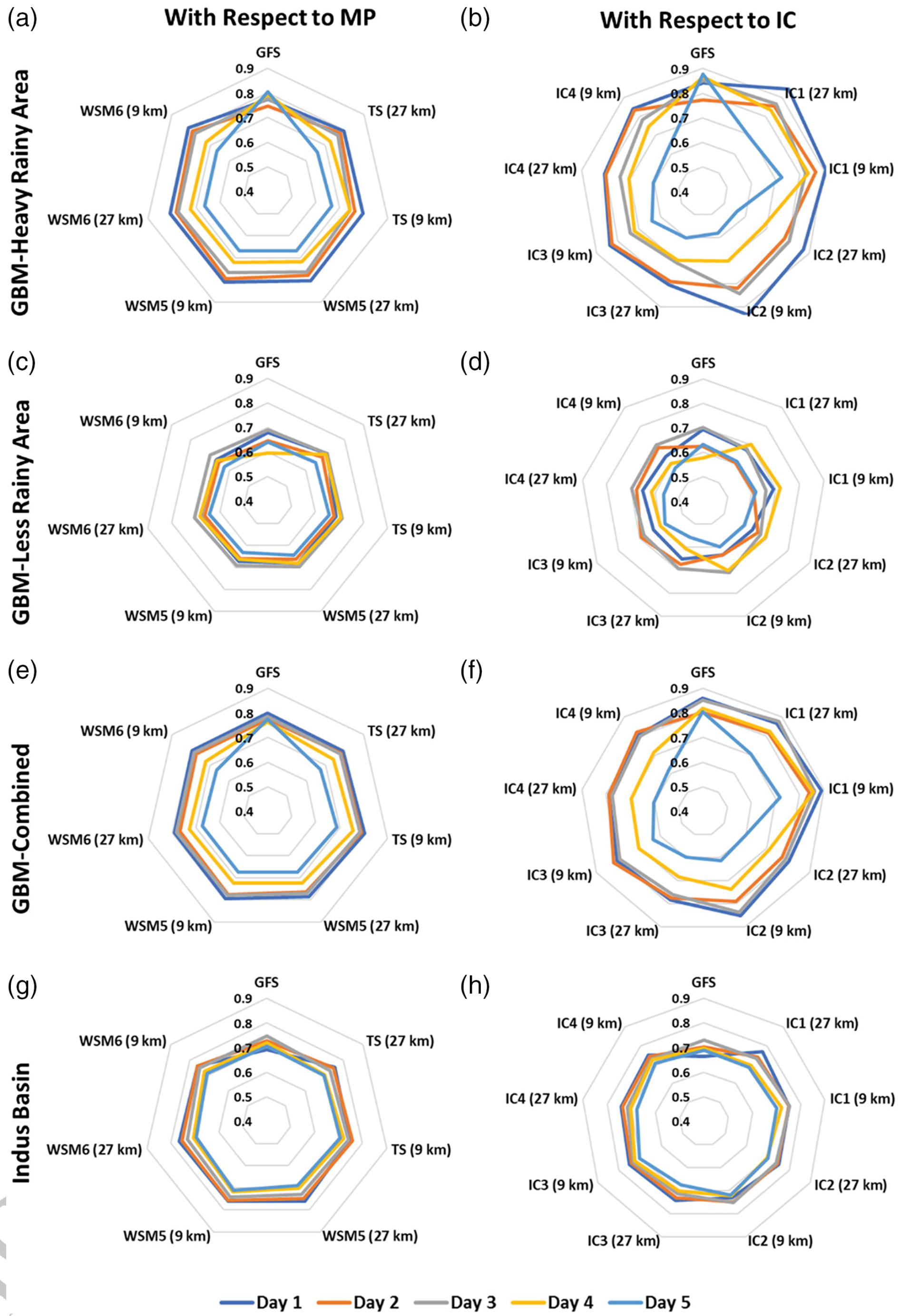

FIGURE 3 Performance (unified score) of the weather research and forecasting (WRF)-forecasted precipitation at different lead times with respect to different microphysics (MP) schemes (a, c, e, g) and initial condition (IC) experiment cases (b, d, f, h). The performance of the quantitative precipitation forecast (QPF) within the heavy rainy area, less rainy area, the combined area of the Ganges–Brahmaputra–Meghna (GBM) basin and within the analysis extent of the Indus basin are shown in the upper, upper-middle, lower-middle and lower panels respectively. Each line represents a lead time. The alternatives (e.g. WRF single moment 6 class (WSM6); IC3) with higher scores (i.e. closer to the circumference) are more accurate [Color figure can be viewed at wileyonlinelibrary.com]

rainy area of the basin. Thus, the outputs of the heavy rainy area revealed the forecast performance during the instance of a rainfall event in that region. On the other hand, the results over the less rainy area provide the performance criteria when the precipitation is sparse or negligible. In the case of the Indus basin, almost the entire basin was considered for the analysis.

At first, the sensitivity of three different cloud MPs on the forecasted precipitation was tested. In the next step, the sensitivity of four different IC test cases on the WRF forecasted precipitation was evaluated. The main objective was to identify the suitable test cases in all conditions of the monsoon-driven South Asian river basins. These analyses were carried out for a few periods (3–6 days depending on the available 1–5 day lead time-simulated forecast) (Table 1). For example, the GBM 2007 storm event was simulated for July 20–26, 2016. Results from a 1 to 5 day lead time were available for each day for July 24–26 for this event. Therefore, these three consecutive days were considered for the IC–MP sensitivity analysis. Likewise, the performance of the simulated daily average wind speed and maximum and minimum temperatures were evaluated with respect to a different IC approach. The impact of using finer resolution data (i.e. the GDAS) as the model IC was then evaluated for the GBM 2015.1 event with respect to different MP schemes and IC approaches. The ability of the

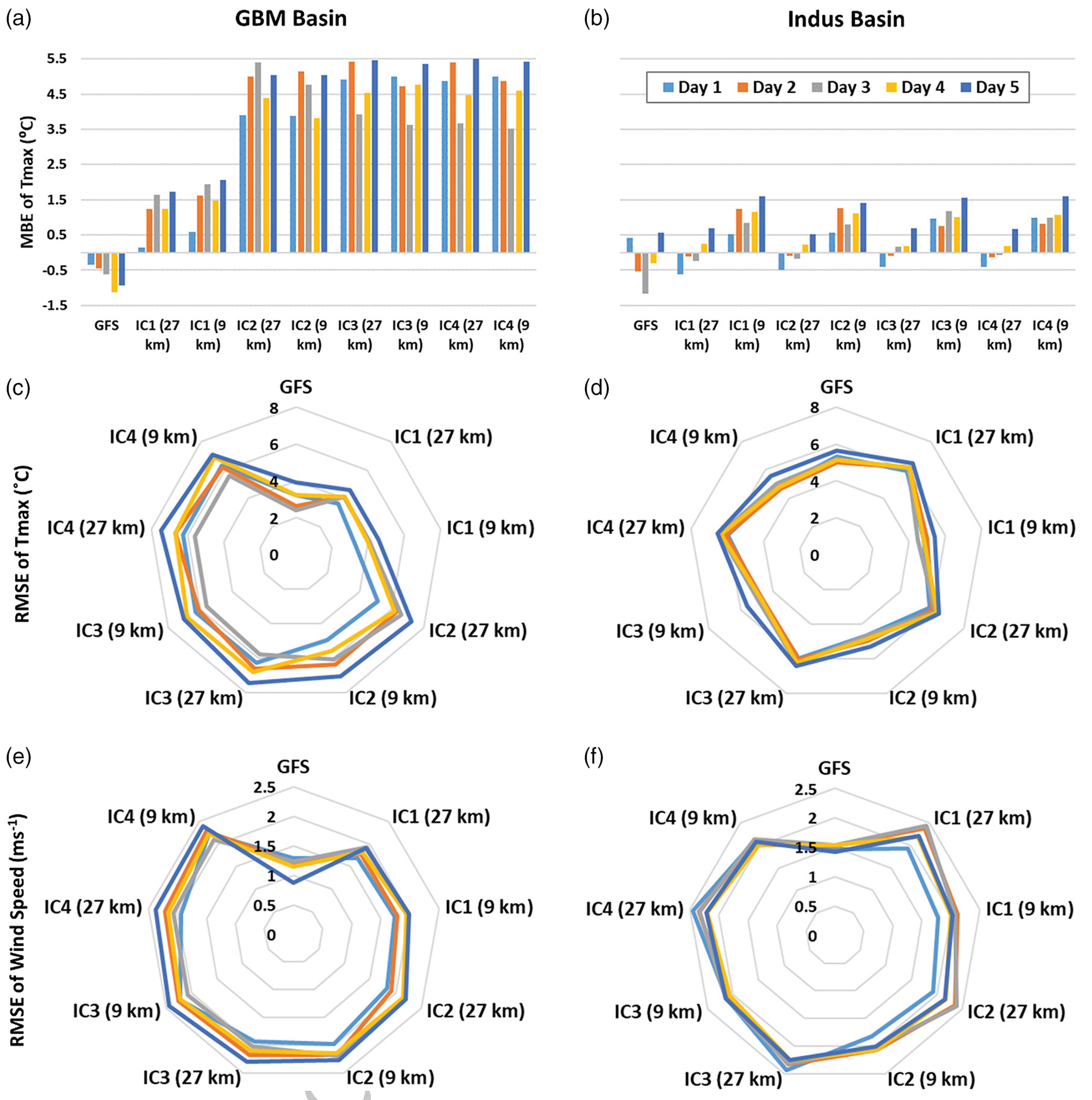

Color online, B&W in print

FIGURE 4 (a, b) Mean bias error (MBE) of the daily maximum temperature (T_{max}); (c, d) root mean squared error (RMSE) of the daily maximum temperature (T_{max}); and (e, f) the RMSE of the daily average wind speed with respect to different initial condition (IC) approaches in the Ganges–Brahmaputra–Meghna (GBM) (e) and Indus basin (f) [Color figure can be viewed at wileyonlinelibrary.com]

model to capture the intense precipitation events was then evaluated. To do so, only the rainiest day of each event was considered. Thus, this analysis was carried out only for one day of each event. Finally, the comparison between the WRF simulated precipitation, temperature and wind speed was carried out using the GFS, GFS-FNL and GDAS-FNL. This analysis assessed the performance of these products to generate the WRF IC. The analysis was performed only for the heavy rainy area of the GBM basin between July 8 and September 31, 2015, based on the common time period of the available data.

To carry out the IC and MP sensitivity tests, categorical and continuous metrics were used. The rescaled error metrics were then calculated using the equations in Table 3. These rescaled metrics ranged from 0 to 1, where 1 is the ideal value in all cases. Finally, the unified score was calculated using Equation (8) to evaluate the overall performance of each combination. In the GBM basin, the GBM 2007 event was simulated using all test scenarios. Along with this event, all three MP schemes in the GBM 2015.1 and GBM 2015.2 events were simulated using only the IC4 test case. Four IC test cases for the GBM 2007 and only the IC4 test case for the GBM 2015.1 and GBM 2015.2 were considered for the analysis of the MP scheme's sensitivity. Thus, the MP scheme's sensitivity analysis in the GBM basin is partially biased by the IC4 test case. On the other hand, all

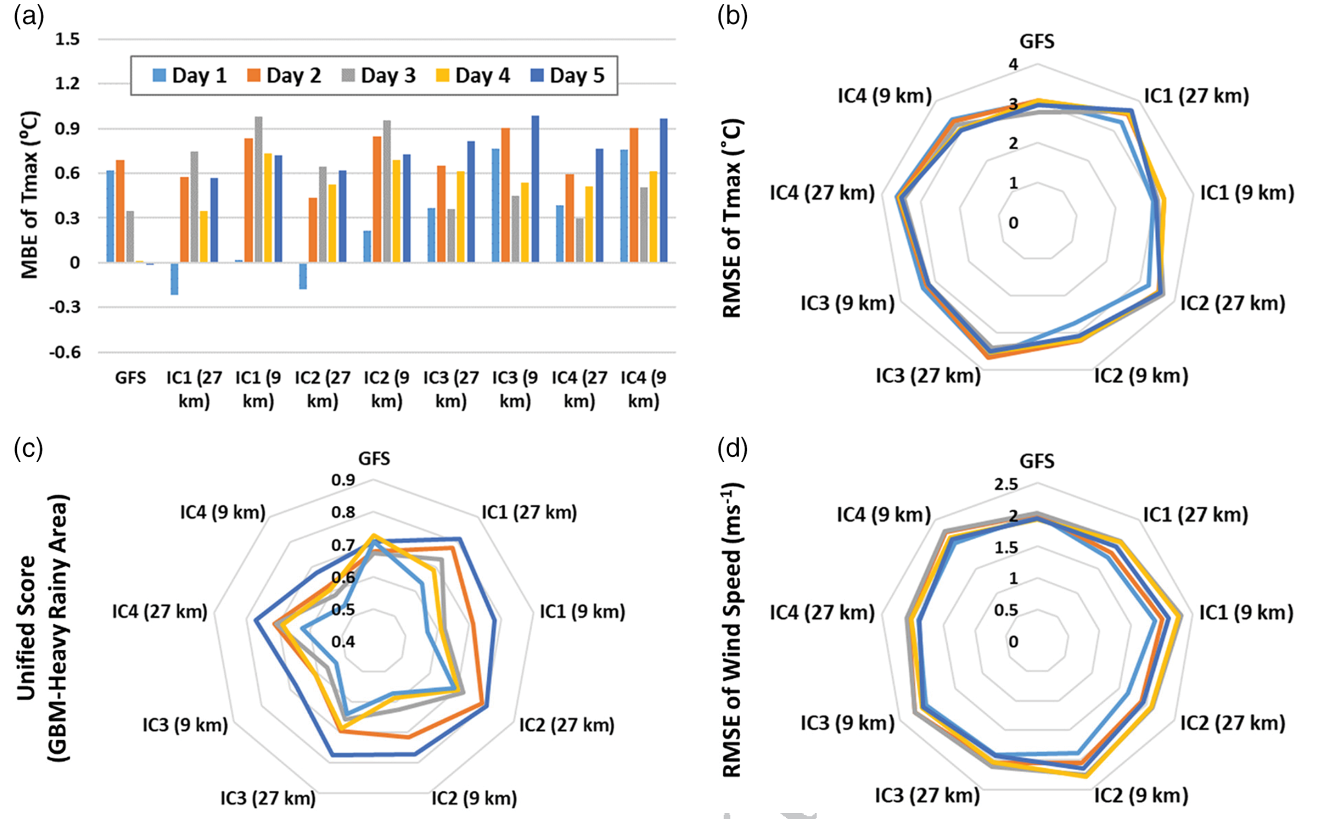

Color online, B&W in print

FIGURE 5 Performance of the daily maximum temperature (T_{max}) (a) mean bias error (MBE) and (b) root mean squared error (RMSE)); (c) weather research and forecasting (WRF)-forecasted precipitation (unified score); and (d) daily average wind speed (RMSE) with respect to different initial condition (IC) approaches in the Ganges–Brahmaputra–Meghna (GBM) basin, considering only the 2015.1 event [Color figure can be viewed at wileyonlinelibrary.com]

three MP schemes of the GBM 2007 were considered for the IC sensitivity test, since the event was simulated for all MP–IC combinations. Though the GBM 2015.1 event was simulated using all the IC test cases with the TS scheme (Table 1), the event was not included in the IC sensitivity test of the GBM basin. This was to be consistent with the Indus basin analysis, where only the Indus 2010 event was considered for the IC sensitivity test. Therefore, this analysis is fully biased by the GBM 2007 event. However, the performance of the IC test cases of the GBM 2015.1 event is shown separately (Figure 5). The number of warm- and cold-start simulations is equal to the Indus basin (Table 1). All simulations were considered for the MP scheme sensitivity test. The simulations of the Indus 2010 event were used for the IC sensitivity test, as all the IC test cases were simulated for this event. Overall, the result of the Indus analysis is partially and fully biased by the performance of the Indus 2010 event in the case of the MP and IC sensitivity tests respectively.

Figure 3 shows the IC–MP sensitivity results. Each line of these radar charts represents a lead time, while each spoke (i.e. radii) represents an alternative (e.g. the IC or MP). The results for both 27 and 9 km domains are shown to evaluate the sensitivity of these variables under different model resolutions. Here the higher score (i.e. the unified score) means a better match with the observations. Thus, the line closer to the circumference of these radar chart means more accuracy; less accurate results are closer to the centre.

The selected MP schemes (Figure 3a) are not that sensitive as the IC approaches (Figure 3b) in the heavy rainy area of the GBM basin. Within this area, the WRF forecasted precipitation with all the MP schemes shows relatively poor performance than the GFS with a higher lead time (Figure 3a). A separate analysis of each event showed that the performance of the GFS in the heavy rainy area of the GBM basin increases with time up to a 5 day lead time, while in the Indus it is up to a 3 day lead time. The performance gradually decreases with time in less rainy areas of the GBM basin. The reason could be the poor quality of the assimilated data in the GFS model. This is discussed further below. The similar performance of all the MP schemes in forecasted precipitation is consistent with the findings of Sikder and Hossain (2016), who reported that these three MP schemes perform equally with the BMJ CP scheme in hindcast mode. The sensitivity analysis of the IC approaches (Figure 3b) suggested that the cold-start options (i.e. the IC1 and IC2) are better than warm start within the wet area of the GBM basin.

Generally, it was expected that the warm (or hot) start should perform better. The reason for this counterintuitive performance was investigated and is discussed below. The performance of the forecasted precipitation is not that sensitive to the MP scheme (Figure 3c) or the IC approach (Figure 3d) within the lesser area of the GBM basin. The reason is that the performance evaluated is based on the number of simulated and observed "rainy" cells. In this area, most of the cells are dry and the analysis only within the less rainy area shows an almost similar performance in all cases. The results of the heavy rainy area are dominant in the combined case; for the same reason as well as the analysis extent of the heavy rainy area is larger than the less rainy area (Figure 3e, f). The Indus basin shows almost a similar response to the different MP schemes (Figure 3g) and IC approaches (Figure 3h). Overall, the WRF forecasted precipitation is not notably sensitive to the selected MP schemes as well as the spatial resolution at this scale. The optimized MP schemes and resolutions identified by Sikder and Hossain (2016) in the hindcast mode for monsoon weather remains true for the forecasting mode. The WRF model shows sensitivity to the IC test cases in the GBM basin as well as in the Indus basin. Here the cold-start IC approaches showed a more promising result than warm start.

Precipitation is a derived variable in the NWP models. Temperature and wind vectors are directly calculated by the primitive equations of the NWP models. Therefore, the performance analysis of the WRF-simulated daily average wind speed and maximum and minimum temperatures was conducted to understand better the sensitivity of the IC approaches. The MBE and RMSE of daily temperature and wind speed are shown in Figure 4. The MBE in the GBM basin (Figure 4a) indicates that the daily maximum temperature (T_{max}) is overestimated by the WRF model. The IC yielded some sensitivity in the case of T_{max} of the GBM basin. On the other hand, the estimated T_{max} is more sensitive to the model resolution than the IC approaches in the Indus basin (Figure 4b). The IC sensitivity analysis is fully biased to the GBM 2007 and Indus 2010 event for the GBM and Indus basin respectively. A separate analysis of the GBM 2015.1 (Figure 5a) shows that the MBE of T_{max} in the GBM basin is also sensitive to the model resolution than the IC, such as the Indus 2010. Thus, the performance shown in Figure 4a is event specific (only in the case of the GBM 2007). The RMSE of T_{max} (Figure 4c, d) shows that at this scale of model resolution the WRF forecasted T_{max} cannot exceed the accuracy of its model boundary (i.e. the GFS). However, the finer resolution model shows a slightly and significantly better result in the GBM and Indus basin respectively. An almost similar performance was found for daily minimum temperature (not shown) and daily average wind speed (Figure 4e, f). The RMSE of T_{max} and wind speed in the GBM 2015.1 event (Figure 5b, d) showed an almost similar performance as the Indus basin. As for precipitation (Figures 3 and 5c), the rather counterintuitive finding of an insignificant improvement in the forecast using the IC3 and IC4 (supposedly a better representation of the IC with assimilated observations) can be attributed to the spatial scale issue. The GFS-FNL is actually available at a 1° resolution, while the cold-start IC fields are at 0.5° resolution. Therefore, it is likely that the coarser scale of the observation-assimilated IC scenarios provides no significant benefit to improving forecast accuracy. This finding regarding the impact of the spatial scale in dynamic downscaling is somewhat consistent with Xiaodong and Hossain (2016). Therefore, the results of the GBM 2015.1 initiated with the GDAS-FNL (0.25°) were compared with the same model initiated with the GFS-FNL in the next step.

The impact of using the fine-resolution IC within the heavy rainy area is shown with respect to different MP schemes (Figure 6a) and different IC approaches (Figure 6b). The analysis of the 9 km domain is reported here, as the impact of the finer IC in the 27 km domain is not significant. This indicates that the use of a finer resolution IC is only suitable in higher resolution models. The use of the GDAS-FNL does not have any positive impact in the case of the WSM5 and WSM5 MP schemes (Figure 6a). However, the difference between the GDAS-FNL and GFS-FNL-initiated model is less in the 9 km domain than in the 27 km domain (not reported). A slight improvement with the TS MP scheme is visible in the lower lead time. Note that only the IC4 test case was considered for this analysis. In the case of different IC approaches (Figure 6b), the impact of using a finer resolution IC is clearly visible, as only the TS scheme was considered. However, Figure 6 reveals that the cold-start approach (here, IC2) significantly improves the result with the GDAS-FNL from a 1 day lead time. In the case of warm starts (i.e. the IC3 and IC4), a late improvement is noticeable. Here the cold-start approach IC2 directly got the IC form GDAS-FNL without any further degradation in quality. The warm starts in this study used a one-day pre-simulation using the available analysis data, seems not reducing the spin-up time error. Instead of reducing any error, the process adds some further uncertainty in the IC through simulation. Therefore, the warm-start approaches used are not worthy for heavy precipitation forecasting in monsoon weather.

Furthermore, each precipitation event was evaluated separately to see the performance of the WRF model at detecting the rainiest day of the events. The performance of different combinations was calculated in terms of accuracy in the spatial distribution using Equation (9), as well as the areal average amount of precipitation. Only the heavy rainy area of the GBM basin was considered for this analysis, while the full basin was considered in the case of the Indus.

Model performance on July 26, 2007 shows that the cold-start case IC1 exhibited better performance in terms of spatial extent as well as in the amount of precipitation (Figure 7a, b) within the heavy rainy area of the GBM basin. The IC4 test case with the TS MP scheme shows

Color online, B&W in print

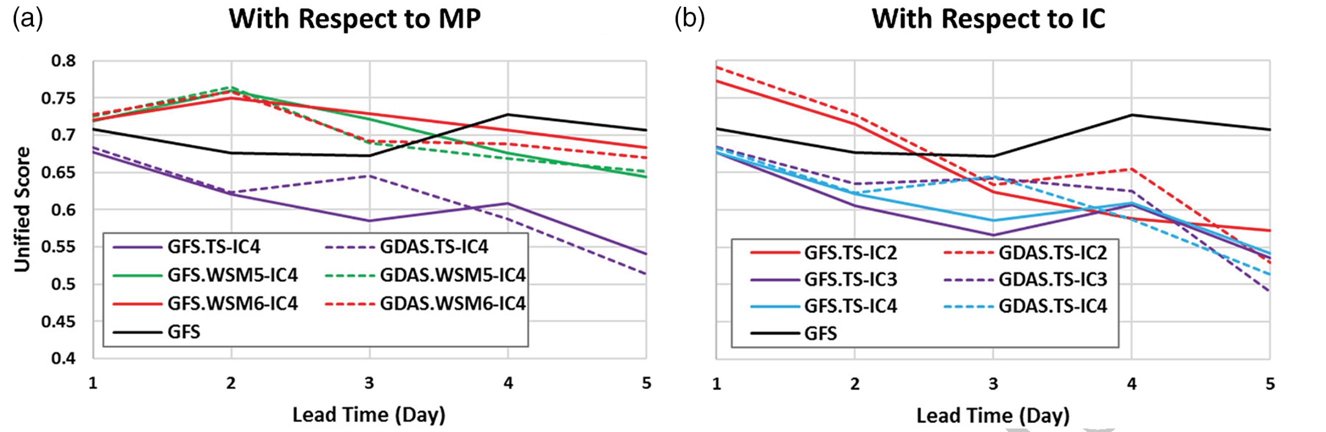

Q17 **FIGURE 6** Comparison between the global forecast system final (GFS-FNL) and global data assimilation system final (GDAS-FNL)-initiated model results with respect to different microphysics (MP) schemes (a) and initial condition (IC) approaches (b). Analyses are shown for the 9 km domain of the heavy rainy area of the Ganges–Brahmaputra–Meghna (GBM) basin [Color figure can be viewed at wileyonlinelibrary.com]

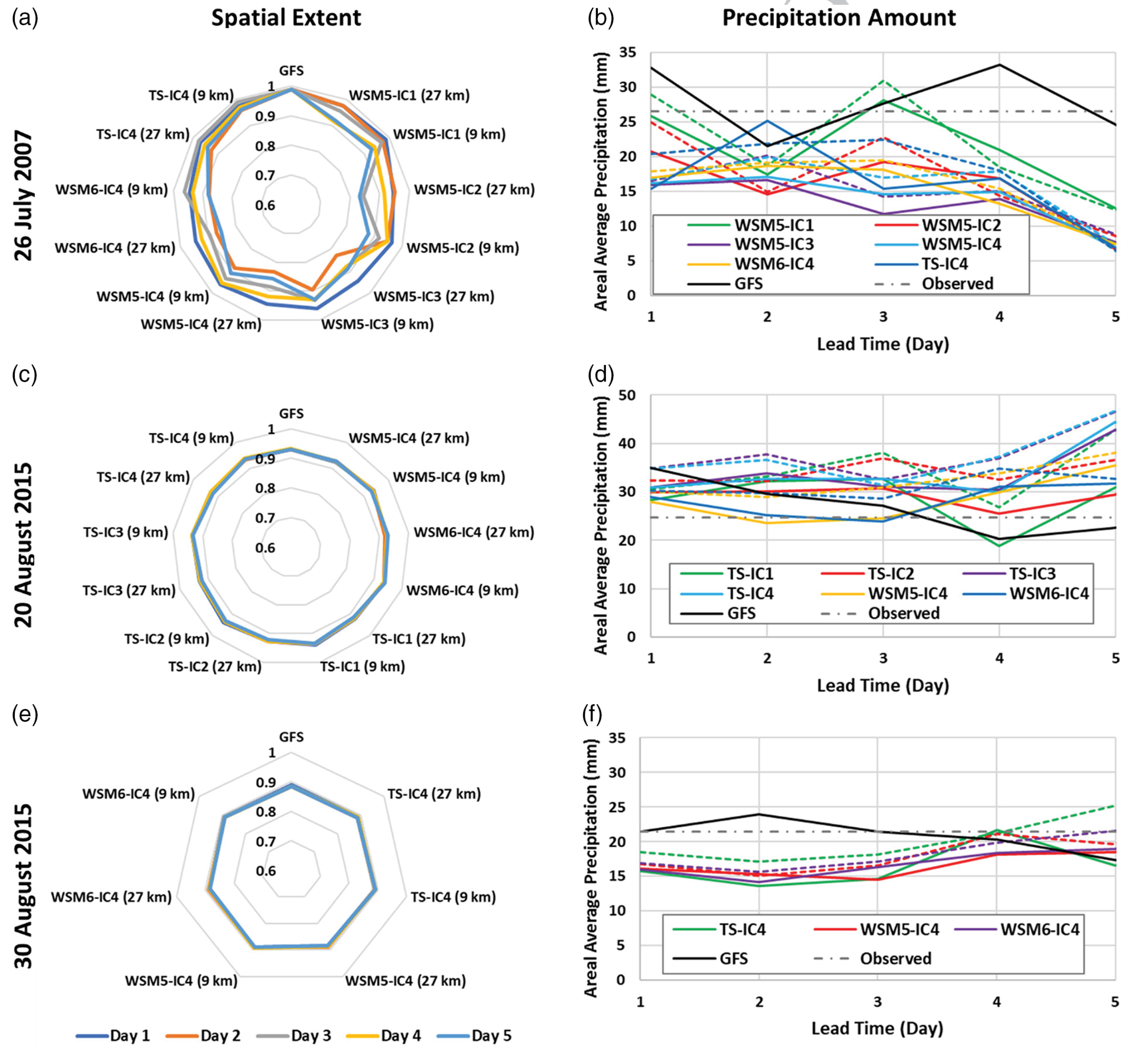

Color online, B&W in print

FIGURE 7 Assessment of forecast accuracy within the heavy rainy area of the Ganges–Brahmaputra–Meghna (GBM) basin in terms of the spatial extent score and as a function of lead time (a, c, e), and in terms of precipitation amount (b, d, f). In (a, c, e), the firm and dashed lines are for results from the 27 and 9 km domains respectively [Color figure can be viewed at wileyonlinelibrary.com]

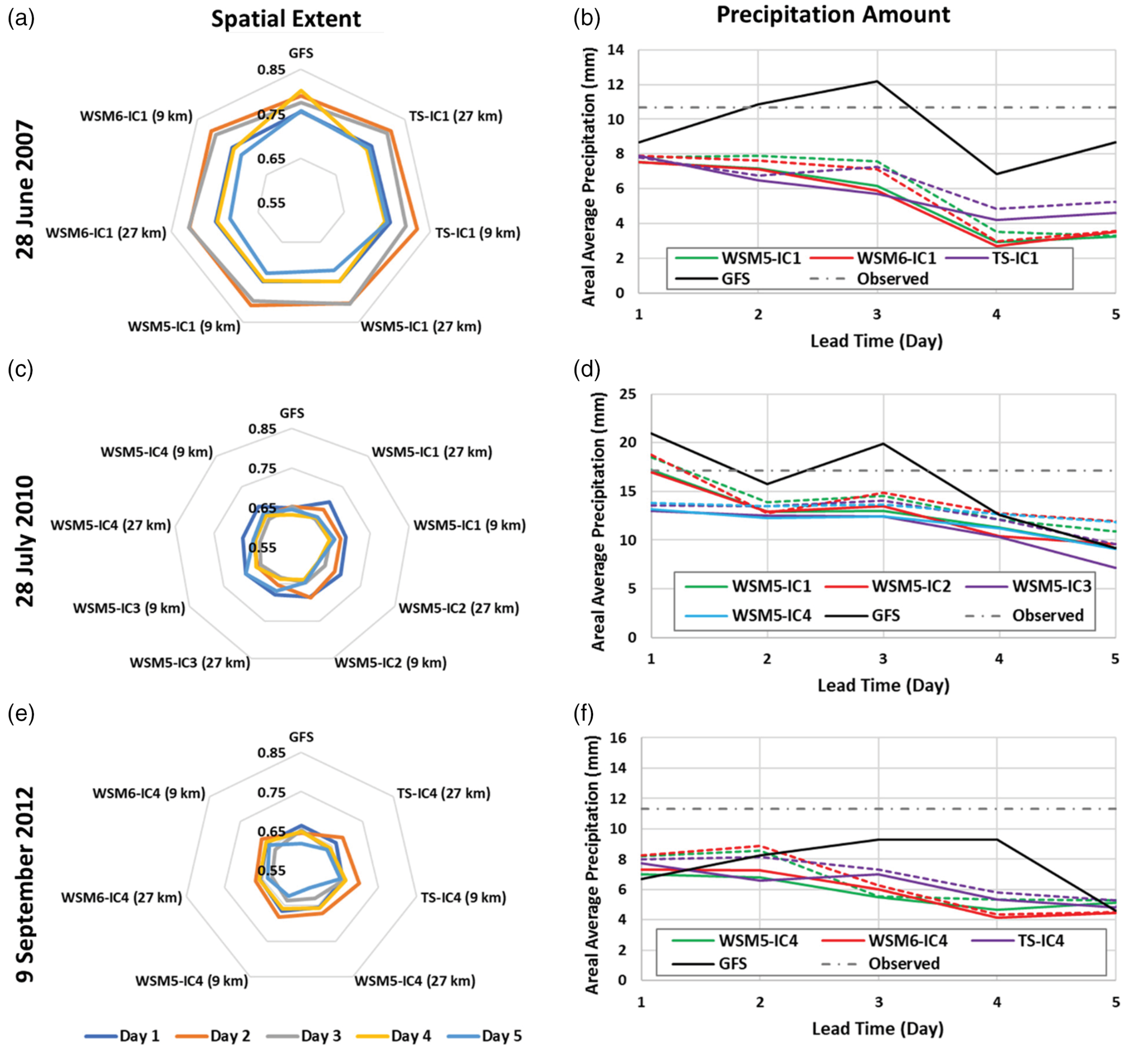

Color online, B&W in print

FIGURE 8 As for Figure 7, but for the Indus basin [Color figure can be viewed at wileyonlinelibrary.com]

slightly better performance in spatial extent score. The accuracy of different combinations in terms of spatial distribution did not vary significantly on August 20, 2015 (Figure 7c). However, in areal average precipitation, the accuracy of the 27 km domain was significantly better than for the 9 km domain (Figure 7d). August 20, 2015 is the only intense event among the selected six days where the WRF simulated precipitation is significantly overestimated. Only the IC4 was tested on August 30 with different MP schemes, where the variation in terms of the spatial extent (Figure 7e) and amount of precipitation (Figure 7f) is not significant. In general, the performance of the WSM5 and WSM6 MP schemes is almost similar and they perform well, particularly with cold-start approaches.

In the Indus basin, the June 28, 2007 event was only tested for the IC1 test case with different MP schemes. The TS scheme shows slightly better performance at higher lead time (after a four-day lead time) both in terms of spatial extent and precipitation amount (Figure 8a, b). July 28, 2010 is the only event where all the MP–IC combinations were tested. However, only the WSM5 with all the IC approaches are reported (Figure 8c, d). The IC1 and IC2 perform better. On September 9, 2012, only the IC4 experiment case was tested, and the TS shows relatively better performance (Figure 8e, f). Overall, the cold-start approaches perform relatively better in the Indus basin like GBM. However, the TS performs slightly better in the Indus basin in case of a heavy rainy day. Q18

The WSM5 and WSM6 are the same MP scheme, except for the graupel in the WSM6. On the other hand, the Thompson scheme is a completely different scheme than both the WSM schemes: it is a single-moment scheme with a double-moment capability in cloud ice variables (Thompson et al., 2008). This is the reason for the Q19

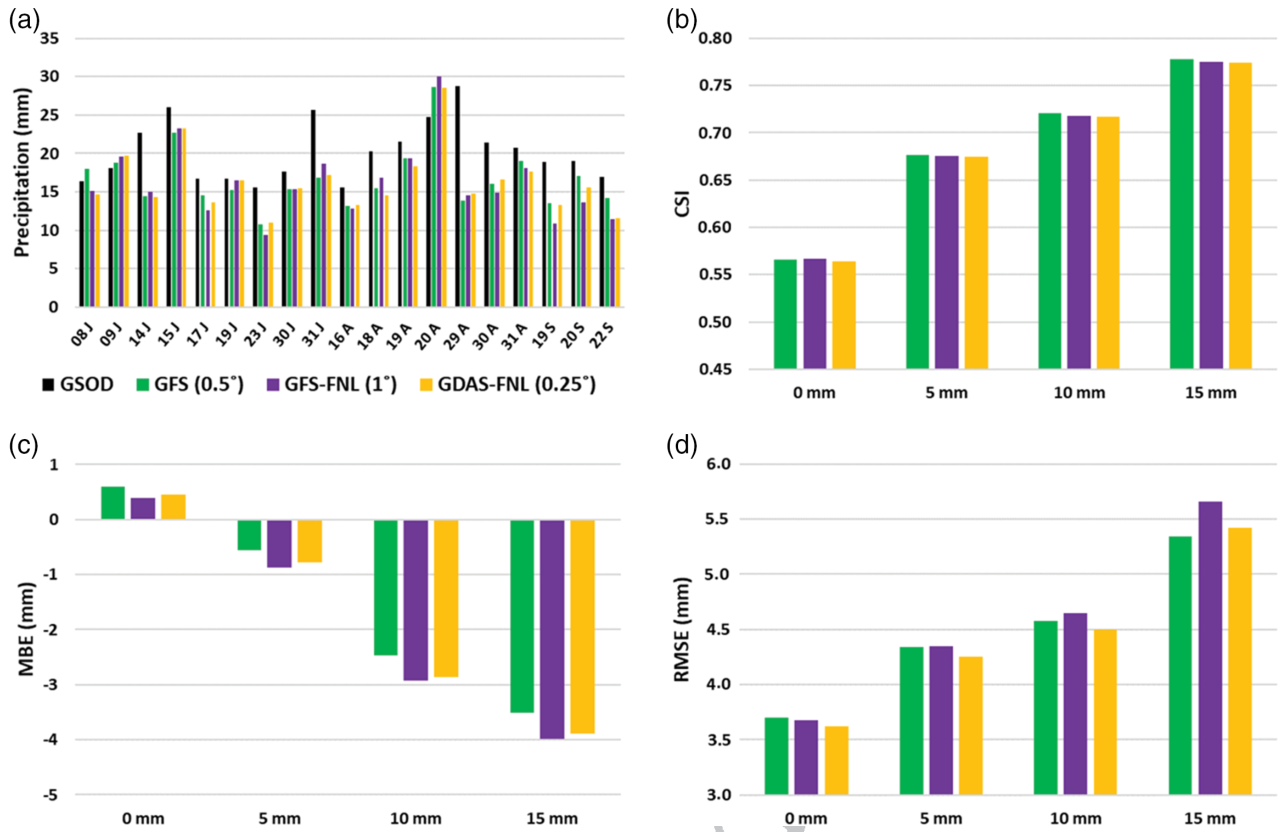

Color online, B&W in print

FIGURE 9 Comparison between the weather research and forecasting (WRF)-simulated precipitation using the global forecast system (GFS), global forecast system final (GFS-FNL) and global data assimilation system final (GDAS-FNL) as the model boundary. Analyses are shown for the 27 km domain of the heavy rainy area of the Ganges–Brahmaputra–Meghna (GBM) basin: (a) precipitation amount, when the observed exceeded 15 mm of rain; (b) critical success index (CSI); (c) mean bias error (MBE); and (d) root mean squared error (RMSE) of the simulated precipitation at different precipitation thresholds [Color figure can be viewed at wileyonlinelibrary.com]

difference in the performance of the WSM schemes with the TS. However, all three MP schemes produced almost similar results within the range of the 9–27 km domains. Thus, the impact of using any sophisticated MP scheme seems unsuitable due to computational time within this scale of model resolution (i.e. 9–27 km). Furthermore, using an MP scheme with graupel (e.g. the WSM6 and TS) is worthy only when the model resolution is below 10 km. Therefore, using the WSM5 scheme up to the 9 km domain is sufficient to generate a precipitation forecast in monsoon weather.

Finally, a comparison between the WRF precipitation using the GFS (0.5°), GFS-FNL (1°) and GDAS-FNL (0.25°) as the model boundary was also performed to investigate the reason behind the poor result in hot-start simulations. The analysis was carried out using different precipitation thresholds (0, 5, 10 and 15 mm) and data from July 8–September 31, 2015. The precipitation is shown in Figure 9a, when the observed precipitation exceeded 15 mm rainfall within the heavy rainy area of the GBM basin. The WRF-simulated precipitation performance was almost equal when using these three products as a model boundary in the case of heavy rainfall (Figure 9a). However, in August and September, the GSF performed consistently better with respect to the others. The CSI (Figure 9b) indicates that the accuracy of the GFS increases with heavier rainfall. A similar trend is visible in the case of the MBE (Figure 9c) and RMSE (Figure 9d), where the GFS shows less error in heavy rainfall (e.g. a 15 mm threshold) than the GFS-FNL and GDAS-FNL as a model boundary. Regardless of the resolution, both final analysis data failed to outperform the GFS in heavy rainfall despite having 10–15% more observed data in their initial state. This indicates that the quality of the assimilated data in the GFS and its final analysis within the ISMR region are inadequate to make a positive impact on predictability, wherein the greater amount of observed data may have introduced more errors into the model product. The error in the observed data is found to be more in the Himalayan foothills, where most of the monsoon rainfall occurs. Since the model accuracy at the lower lead times is more dependent on the model IC than the boundary, inadequate data assimilation can also be the reason behind the inverse trend of the GFS forecast as a function of lead time in the heavy rainy area of the GBM basin.

7 | CONCLUSIONS

The major goal of this study was the assessment of the sensitivity of different model-initializing techniques (initial condition — IC) and cloud microphysics (MP) on the accuracy of the weather research and forecasting (WRF) forecasted precipitation of South Asia. A total of six events including an intense rainy day in the Ganges–Brahmaputra–Meghna (GBM) and Indus River basin were tested to identify the most suitable microphysics–initial condition (MP–IC) combination for the flood forecaster. Although the six events studied may not be enough to generalize the findings, this study does provide some suggestions for further studies with similar objectives. From the results of this study, the authors have attempted to present a general guideline to predict rainfall more accurately using the WRF model in the monsoon-driven climate regime. Such a guideline can be helpful for the flood-forecasting agencies of South Asian countries where the Indian summer monsoon rainfall (ISMR) is the governing reason for flooding.

The primary conclusion is that the warm-start options designed for this study cannot significantly outperform the cold-start options. In most cases, the cold-start shows better performance than the warm-start options. From a comparison of the global data assimilation system final (GDAS-FNL) and global forecast system final (GFS-FNL)-initiated models, it seems that the one-day pre-simulation (hindcast simulation) of warm-start options does not remove the spin-up time error. Rather, this pre-simulation process adds further uncertainty in the model IC. The same comparison analysis reveals that the use of higher-resolution IC with a simple cold-start option may improve forecast performance. A similar finding has been reported for the model boundary resolution for the Indian subcontinent by Kumar, Kishtawal, and Pal (2016). However, the straightforward comparison between the GFS, GFS-FNL and GDAL-FNL indicates there is the possibility of poor-quality data assimilation in the GFS and GFS final analysis products in the Himalayan foothills region. This is the reason for the relatively poor result in the GFS final analysis products, where 10–15% more observed data are used through assimilation. Ultimately, this forcing error propagated in the warm-start test cases designed for this study, where the GFS final analysis products were used to generate the WRF IC.

In the case of cloud MP, the performance of the WRF single moment 5 class (WSM5) and WRF single moment 6 class (WSM6) MP schemes is mostly similar. These MP schemes perform well with cold-start options. The WSM schemes show their consistency in the case of the heavy rainy days within the GBM basin. On the other hand, the Thompson scheme (TS) MP scheme seems to work well in the heavy rainy days of the Indus basin, no matter what is the IC case. However, the difference between the WSM and TS schemes in not that significant at this scale. Thus, considering the computational requirement of a complex MP, it can be concluded that the WSM5 is the recommended option with the cold-start IC approach at this scale. The sensitivity of the MP schemes shows consistency with the findings of Sikder and Hossain (2016).

ACKNOWLEDGEMENTS

This study was supported by a NASA WATER grant (number NNX15AC63G). The first author was supported by a NASA Earth and Space Fellowship (number NNX16 AO68H).

REFERENCES

Alam, M. M. (2014). Impact of cloud microphysics and cumulus parameterization on simulation of heavy rainfall event during 7–9 October 2007 over Bangladesh. *Journal of Earth System Science*, *123*(2), 259–279.

Bei, N., & Zhang, F. (2007). Impacts of initial condition errors on mesoscale predictability of heavy precipitation along the Mei-Yu front of China. *Quarterly Journal of the Royal Meteorological Society*, *133*(622), 83–99.

Bhaskaran, B., Jones, R. G., Murphy, J. M., & Noguer, M. (1996). Simulations of the Indian summer monsoon using a nested regional climate model: Domain size experiments. *Climate Dynamics*, *12*(9), 573–587.

Bray, M., Han, D., Xuan, Y., Bates, P., & Williams, M. (2011). Rainfall uncertainty for extreme events in NWP downscaling model. *Hydrological Processes*, *25*(9), 1397–1406.

Castro, C. L., Pielke Sr., R. A., & Leoncini, G. (2005). Dynamical downscaling: Assessment of value retained and added using the Regional Atmospheric Modeling System (RAMS). *Journal of Geophysical Research*, *110*(D05108). https://doi.org/10.1029/2004JD004721

Cuo, L., Pagano, T. C., & Wang, Q. J. (2011). A review of quantitative precipitation forecasts and their use in short- to medium-range streamflow forecasting. *Journal of Hydrometeorology*, *12*(5), 713–728.

Dudhia, J. (1989). Numerical study of convection observed during the Winter Monsoon Experiment using a mesoscale two–dimensional model. *Journal of Atmospheric Sciences*, *46*(20), 3077–3107. https://doi.org/10.1175/1520-0469(1989)046<3077:NSOCOD>2.0.CO;2

Dulal, H. B. (2014). Governing climate change adaptation in the Ganges basin: Assessing needs and capacities. *International Journal of Sustainable Development & World Ecology*, *21*(1), 1–14.

Durai, V. R., & Bhardwaj, R. (2013). Improving precipitation forecasts skill over India using a multi-model ensemble technique. *Geofizika*, *30*(2), 119–141.

Dwivedi, S., Mittal, A. K., & Goswami, B. N. (2006). An empirical rule for extended range prediction of duration of Indian summer monsoon breaks. *Geophysical Research Letters*, *33*(L18801), 1–5. https://doi.org/10.1029/2006GL027035

Ebert, E. E. (2001). Ability of a poor man's ensemble to predict the probability and distribution of precipitation. *Monthly Weather Review*, *129*, 2461–2480.

FAO. (2011). *AQUASTAT*. Retrieved from http://www.fao.org/nr/water/aquastat/main/index.stm

Georgakakos, K. P., Graham, N. E., Modrick, T. M., Murphy Jr., M. J., Shamir, E., Spencer, C. R., & Sperfslage, J. A. (2014). Evaluation of real-time hydrometeorological ensemble prediction on hydrologic scales in Northern California. *Journal of Hydrology*, *519*, 2978–3000.

Givati, A., Lynn, B., Liu, Y., & Rimmer, A. (2012). Using the WRF model in an operational streamflow forecast system for the Jordan River. *Journal of Applied Meteorology and Climatology*, *51*, 285–299.

Hong, S. Y., Dudhia, J., & Chen, S. H. (2004). A revised approach to ice microphysical processes for the bulk parameterization of clouds and precipitation. *Monthly Weather Review*, *132*, 103–120. https://doi.org/10.1175/1520-0493(2004)132<0103:ARATIM>2.0.CO;2

Hong, S. Y., & Lim, J. O. J. (2006). The WRF single-moment 6-class microphysics scheme (WSM6). *Journal of the Korean Meteorological Society*, *42*(2), 129–151.

Hong, S. Y., Noh, Y., & Dudhia, J. (2006). A new vertical diffusion package with an explicit treatment of entrainment processes. *Monthly Weather Review*, *134*, 2318–2341. https://doi.org/10.1175/MWR3199.1

Houze Jr., R. A., Rasmussen, K. L., Medina, S., Brodzik, S. R., & Romatschke, U. (2011). Anomalous atmospheric events leading to the summer 2010 floods in Pakistan. *Bulletin of the American Meteorological Society*, *92*(3), 291–298.

Hsiao, L. F., Yanga, M. J., Leea, C. S., Kuoa, H. C., Shiha, D. S., Tsaia, C. C., … Lina, W. F. (2013). Ensemble forecasting of typhoon rainfall and floods over a mountainous watershed in Taiwan. *Journal of Hydrology*, *506*, 55–68.

Huffman GJ. (2013). *Algorithm 3B42: TRMM merged HQ/infrared precipitation*. Retrieved from http://trmm.gsfc.nasa.gov/3b42.html

Islam, A. K. M. S., Haque, A., & Bala, S. K. (2010). Hydrologic characteristics of floods in Ganges–Brahmaputra–Meghna (GBM) delta. *Natural Hazards*, *54*(3), 797–811.

Jang, J., & Hong, S. Y. (2014). Quantitative forecast experiment of a heavy rainfall event over Korea in a global model: Horizontal resolution versus lead time issues. *Meteorology and Atmospheric Physics*, *124*(3), 113–127.

Janjic, Z. I. (1994). The Step–Mountain Eta Coordinate Model: Further developments of the convection, viscous sublayer, and turbulence closure schemes. *Monthly Weather Review*, *122*, 927–945. https://doi.org/10.1175/1520-0493(1994)122<0927:TSMECM>2.0.CO;2

Jankov, I., Gallus Jr., W. A., Segal, M., & Koch, S. E. (2007). Influence of initial conditions on the WRF-ARW Model QPF response to physical parameterization changes. *Weather and Forecasting*, *22*(3), 501–519.

Kale, V. (2012). On the link between extreme floods and excess monsoon epochs in South Asia. *Climate Dynamics*, *39*(5), 1107–1122.

Kalnay, E. (2003). *Atmospheric modeling, data assimilation, and predictability*. New York, NY: Cambridge University Press.

Kumar, P., Kishtawal, C. M., & Pal, P. K. (2015). Impact of ECMWF, NCEP, and NCMRWF global model analysis on the WRF model forecast over Indian Region. *Theoretical and Applied Climatology*. https://doi.org/10.1007/s00704-015-1629-1

Kumar, P., Kishtawal, C. M., & Pal, P. K. (2016). Skill of regional and global model forecast over Indian region. *Theoretical and Applied Climatology*, *123*(3), 629–636. https://doi.org/10.1007/s00704-014-1361-2

Kumar, R. A., Dudhia, J., & Bhowmik, S. K. R. (2010). Evaluation of Physics options of the Weather Research and Forecasting (WRF) Model to simulate high impact heavy rainfall events over Indian Monsoon region. *Geofizika*, *27*(2), 101–125.

Liu, J., Bray, M., & Han, D. (2012). Sensitivity of the Weather Research and Forecasting (WRF) model to downscaling ratios and storm types in rainfall simulation. *Hydrological Processes*, *26*, 3012–3031.

Lorenz, E. (1963). Deterministic non-periodic flows. *Journal of Atmospheric Sciences*, *20*, 130–141.

Medina, S., Houze Jr., R. A., Kumar, A., & Niyogi, D. (2010). Summer monsoon convection in the Himalayan region: Terrain and land cover effects. *Quarterly Journal of the Royal Meteorological Society*, *136*(648), 593–616.

Memon, A. A., Muhammad, S., Rahman, S., & Haq, M. (2015). Flood monitoring and damage assessment using water indices: A case study of Pakistan flood-2012. *The Egyptian Journal of Remote Sensing and Space Sciences*, *18*(1), 99–106.

Mirza, M. M. Q. (2011). Climate change, flooding in South Asia and implications. *Regional Environmental Change*, *11*(Suppl. 1), 95–107.

Mlawer, E. J., Taubman, S. J., Brown, P. D., Iacono, M. J., & Clough, S. A. (1997). Radiative transfer for inhomogeneous atmospheres: RRTM, a validated correlated–k model for the longwave. *Journal of Geophysical Research*, *102*(D14), 16663–16682. https://doi.org/10.1029/97JD00237

Molden, D. (2007). In D. Molden (Ed.), *Water for food, water for life*. London, England: Earthscan and International Water Management Institute: Colombo, Sri Lanka.

Mukhopadhyay, P., Taraphdar, S., Goswami, B. N., & Krishnakumar, K. (2010). Indian summer monsoon precipitation climatology in a high resolution regional climate model: Impacts of convective parameterization on systematic biases. *Weather and Forecasting*, *25*(2), 369–387. https://doi.org/10.1175/2009WAF2222320.1

Nam, D. H., Mai, D. T., Udo, K., & Mano, A. (2014). Short-term flood inundation prediction using hydrologic-hydraulic models forced with downscaled rainfall from global NWP. *Hydrological Processes*, *28*, 5844–5859.

Paulikas, M. J., & Rahman, M. K. (2015). A temporal assessment of flooding fatalities in Pakistan (1950–2012). *Journal of Flood Risk Management*, *8*(1), 62–70.

Raju, A., Parekh, A., Kumar, P., & Gnanaseelan, C. (2015). Evaluation of the impact of AIRS profiles on prediction of Indian summer monsoon using WRF variational data assimilation system. *Journal of Geophysical Research: Atmospheres*, *120*(16), 8112–8131.

Rakesh, V., Singh, R., Pal, P. K., & Joshi, P. C. (2007). Sensitivity of mesoscale model forecast during a satellite launch to different cumulus parameterization schemes in MM5. *Pure and Applied Geophysics*, *164*(8), 1617–1637.

Rakesh, V., Singh, R., Pal, P. K., & Joshi, P. C. (2009). Impacts of satellite-observed winds and total precipitable water on WRF short-range forecasts over the Indian region during the 2006 summer monsoon. *Weather and Forecasting*, *24*(6), 1706–1731.

Rakesh, V., Singh, R., Yuliya, D., Pal, P. K., & Joshi, P. C. (2009). Impact of variational assimilation of MODIS thermodynamic profiles in the simulation of western disturbance. *International Journal of Remote Sensing*, *30*(18), 4867–4887.

Ratnam, J. V., & Cox, E. A. (2006). Simulation of monsoon depressions using MM5: Sensitivity to cumulus parameterization schemes. *Meteorology and Atmospheric Physics*, *93*(1), 53–78.

Roberts, N. M., Cole, S. J., Forbes, R. M., Moore, R. J., & Boswell, D. (2009). Use of high-resolution NWP rainfall and river flow forecasts for advance warning of the Carlisle flood, north-west England. *Meteorological Applications*, *16*, 23–34.

Roberts, N. M., & Lean, H. W. (2008). Scale-selective verification of rainfall accumulations from high-resolution forecasts of convective events. *Monthly Weather Review*, *136*(1), 78–97.

Routray, A., Mohanty, U. C., Rizvi, S. R. H., Niyogi, D., Osuri, K. K., & Pradhan, D. (2010). Impact of Doppler weather radar data on numerical forecast of Indian monsoon depressions. *Quarterly Journal of the Royal Meteorological Society*, *136*(652), 1836–1850.

Sikder, S., & Hossain, F. (2016). Assessment of the weather research and forecasting model generalized parameterization schemes for advancement of precipitation forecasting in monsoon-driven river basins. *Journal of Advances in Modeling Earth Systems*, *8*, 1210–1228. https://doi.org/10.1002/2016MS000678

Sikka, R. D., & Rao, P. S. (2008). The use and performance of mesoscale models over the Indian region for two high-impact events. *Natural Hazards*, *44*(3), 353–372.

Skamarock, W. C., Klemp, J. B., Dudhia, J., Gill, D. O., Barker, D. M., Duda, M. G., …, Powers, J. G. (2008). *A description of the advanced research WRF Version 3* (NCAR Technical Note: NCAR/TN-4751STR). Boulder, CO: NCAR.

Sowjanya, K., Kar, S. C., Routray, A., & Mali, P. (2013). Impact of SSM/I retrieval data on the systematic bias of analyses and forecasts of the Indian summer monsoon using WRF assimilation system. *International Journal of Remote Sensing*, *34*(2), 631–654.

Srinivas, C. V., Hariprasad, D., Rao, D. V. B., Anjaneyulu, Y., Baskaran, R., & Venkatraman, B. (2013). Simulation of the Indian summer monsoon regional climate using advanced research WRF model. *International Journal of Climatology*, *33*(5), 1195–1210. https://doi.org/10.1002/joc.3505

Srinivas, C. V., Prasad, D. H., Rao, D. V. B., Baskaran, R., & Venkatraman, B. (2015). Simulation of the Indian summer monsoon onset-phase rainfall using a regional model. *Annales Geophysicae*, *33*(9), 1097–1115.

Tewari, M., Chen, F., Wang, W., Dudhia, J., LeMone, M. A., Mitchell, K., …, Cuenca, R. H. (2004). *Implementation and verification of the unified NOAH land surface model in the WRF model.* Proceedings of 20th Conference on Weather Analysis and Forecasting/16th Conference on Numerical Weather Prediction, Seattle, WA. American Meteorological Society: Boston, MA.

Thompson, G., Field, P. R., Rasmussen, R. M., & Hall, W. D. (2008). Explicit forecasts of winter precipitation using an improved bulk microphysics scheme. Part II: Implementation of a new snow parameterization. *Monthly Weather Review*, *136*, 5095–5115. https://doi.org/10.1175/2008MWR2387.1

Vaidya, S. S. (2006). The performance of two convective parameterization schemes in a mesoscale model over the Indian region. *Meteorology and Atmospheric Physics*, *92*(3), 175–190.

Wang, S. Y., Davies, R. E., Huang, W. R., & Gillies, R. R. (2011). Pakistan's two-stage monsoon and links with the recent climate change. *Journal of Geophysical Research: Atmospheres*, *116*(D16114), 1–15.

World Bank. (2007). *Pakistan - Cyclone and floods 2007: Preliminary damage and needs assessment - Balochistan and Sindh*. Washington, DC: World Bank. Retrieved from http://documents.worldbank.org/curated/en/606211468058511720/Pakistan-Cyclone-and-floods-2007-preliminary-damage-and-needs-assessment-Balochistan-and-Sindh

Xiaodong, C., & Hossain, F. (2016). Revisiting extreme storms of the past 100 years for future safety of large water management infrastructures. *Earth's Future*, *4*(7). https://doi.org/10.1002/2016EF000368

Yucel, I., & Onen, A. (2014). Evaluation a mesoscale atmosphere model and a satellite-based algorithm in estimating extreme rainfall events in northwestern Turkey. *Natural Hazards and Earth System Sciences*, *14*, 611–624.

Zhang, D., & Anthes, R. A. (1982). A high–resolution model of the planetary boundary layer– sensitivity tests and comparisons with SESAME–79 data. *Journal of Applied Meteorology and Climatology*, *21*, 1594–1609. https://doi.org/10.1175/1520-0450(1982)021<1594:AHRMOT>2.0.CO;2

How to cite this article: Sikder MS, Hossain F. Sensitivity of initial-condition and cloud microphysics to the forecasting of monsoon rainfall in South Asia. *Met. Apps*. 2018;1–18. https://doi.org/10.1002/met.1716